Isotope and Pressure Dependence of Liquid−Liquid Equilibria in Polymer Solutions. 7. Solute and Solvent H/D Isotope Effects in Polystyrene−Propionitrile Solutions

Marek Luszczyk[†] and W. Alexander Van Hook*

Chemistry Department, University of Tennessee, Knoxville, Tennessee 37996-1600

Received November 21, 1995; Revised Manuscript Received June 17, 1996[⊗]

ABSTRACT: Cloud and spinodal loci have been obtained as functions of pressure (P), temperature (T), polymer segment number (r), segment fraction (ψ), and H/D substitution on solute (z_D) or solvent (y_D) for polystyrene-*h*/propionitrile-*h* (PSh/PNh) solutions, polystyrene-*h*/propionitrile-2,2-d_2 solutions (PSh/PNd), and polystyrene-*d*/propionitrile-*h* solutions (PSd/PNh). A light scattering technique was employed. An increase in pressure or an increase in the H/D ratio in the solvent (or decrease in the polymer H/D ratio) increases the region of miscibility. The solutions show upper and lower branches which may join at hypercritical points depending on the pressure, molecular weight, or solvent H/D ratio. A least-squares technique to fit experimental data to the continuous mean-field thermodynamic description of polymer−solvent demixing developed by Luszczyk, Rebelo, and Van Hook (*Macromolecules* **1995**, *28*, 745) is described and then illustrated by application to the PS/PN data.

1. Introduction

Polymer miscibility is of interest because the conditions for phase equilibrium are sensitive to the details of the free energy surface. Therefore demixing data can be used to test mean-field models for polymer solutions. Also the physical properties of polymer blends and solutions depend sensitively on phase equilibria in the mixture. For these reasons, Van Hook and co-workers[1−6] have instituted a program exploring the effects of isotope substitution, concentration, pressure, molecular weight, and solvent character on demixing in polymer/polymer and polymer/solvent systems. The present paper reports on two steps toward the realization of this program. First, it describes cloud and spinodal point measurements for polystyrene/propionitrile (PS/PN) solutions. PS/PN is a good example of a system of intermediate solvent quality. The transition from Θ to non-Θ solvent for PN can be controlled by varying pressure and/or isotope substitution. Second, we describe the development of a least-squares technique to fit experimental phase equilibrium data (like that for PS/PN) to the continuous mean-field thermodynamic description of polymer−solvent demixing presented earlier.[4] That model takes full account of polydispersity, calculates cloud and shadow concentrations and spinodal conditions, and includes a treatment of pressure, isotope, and molecular weight dependences. The free energy surface is extremely flat in the vicinity of the equilibrium conditions and convergence is slow. Therefore the development of a least squares routine operating with an acceptable compute time employing 486 PC equipment required a new approach.

2. Experimental Section

Equipment and Technique. The data reported in this paper were obtained using equipment and techniques described previously.[1,2,4] The solutions are contained in Pyrex capillaries. Pressure ($0 \le P$/MPa ≤ 7) and temperature ($272 \le T$/K ≤ 473) are under computer control, and pressure/time and/or temperature/time profiles are programmable. Pressure is transmitted hydraulically to the samples via a mercury seal, and cloud and spinodal points are detected by a light scattering technique.[1,4,7]

In the region of the phase diagram of interest, PS/PN solutions are characterized by upper and lower consolute branches separated by a homogeneous one-phase region (see Figure 1). The most convenient way to determine cloud and spinodal points using the apparatus is to first place the sample into the homogeneous region at elevated pressure, then induce precipitation by lowering pressure, all the while monitoring low-angle scattering intensity. It is more efficient to induce a phase change by varying pressure than temperature because the high thermal mass of the cell and thermostat results in a thermal relaxation time which is many times longer than the pressure relaxation time, but we have carried out some experiments changing temperature instead of pressure. The observed scattering intensities are corrected for stray reflection and multiple scattering. The cloud point (CP) locus is equated to that point on $1/I_{corr}$ *vs* P (or T) least squares fits where the slope changes abruptly, and the operational spinodal (SP) is assigned to the $1/I_{corr} = 0$ intercept.[2,4,7] This laborious procedure for data workup is not always necessary. For strong scatterers, the marked kink in $1/I_{corr}$ plots found at the cloud point is manifested by an equally strong kink in uncorrected (I_{sc},P) or (I_{sc},T) plots. These are routinely plotted by the computer controlling the experiment, and CP loci can be picked directly from the plots of raw data with little or no loss in accuracy. Examples are given in the supplemental data tables. We typically measured T *vs* P isopleths on a given sample with a precision of ±0.01 K and ±0.01 MPa. Measurements were made on samples of six different MW's at about eight different concentrations per sample; duplicate runs were made at many concentrations. The resulting data net consists of about 1150 cloud and spinodal data points generated from the least squares fits of the corrected intensity data (CP_{lsq} and SP_{lsq}), and a corresponding set of approximate cloud points (CP_{apr}) (*i.e.* visually "picked off" plots of the raw data). Each CP_{lsq}, SP_{lsq}, or CP_{apr} dependent variable corresponds to a set of independent variables including temperature (T), pressure (P), molecular weight (MW), polymer polydispersity ($\rho = M_w/M_n$), and isotope label on solvent or polymer (y_D = fraction of D-labeled solvent, z_D = fraction of D-labeled polymer). In almost every case, CP_{apr} is within ≈0.05 MPa of CP_{lsq} (or, reexpressed in terms of the equivalent thermal variation, within ≈0.05 K). A list of the temperature and pressure ranges and the concentrations, polydispersities, and isotope labeling for each isopleth is given in Table 1. The entire data net is reported in the supplemental material.

* To whom correspondence should be addressed.
[†] Permanent address: Institute of Physical Chemistry, Polish Academy of Sciences, Warsaw.
[⊗] Abstract published in *Advance ACS Abstracts,* September 1, 1996.

S0024-9297(95)01730-X CCC: $12.00

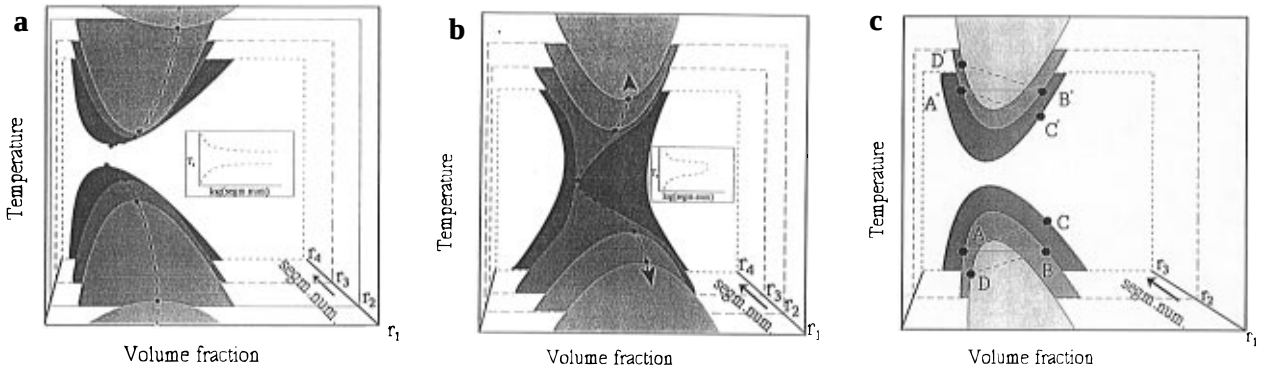

Figure 1. Schematics for UCST/LCST demixing in $(T,\psi,r)_P$ space. ψ is the segment fraction, and r the segment number. The upper and lower branches of the two-phase regions are shaded. Skewing in the (T,ψ) plane is understood in terms of Flory–Huggins theory. The phase diagram in $(T,\psi,P)_r$ space is analogous to this Figure except that fractionation in P is impossible. Also P decreases as one moves into the page. (a) For solutions in good solvents (like methylcyclohexane/polystyrene) which show upper and lower Θ points. The inset shows the projection of critical lines at several pressures onto the $(T,\log(r))$ plane. (b) For non-Θ solutions (like propionitrile/polystyrene) which show upper and lower branches which join at a hypercritical point. The inset shows the projection of critical lines onto the $(T,\log(r))$ plane. The hypercritical point is shown as the solid circle at the center. (c) Several sections from (a) or (b) chosen to illustrate the origin of MW fractionation in liquid–liquid equilibria of polydisperse polymer solutions. The equilibria shown are between A and C, A′ and C′, B and D, and B′ and D′. The cloud point curves (heavy solid line) are flat in the region of the maximum or minimum, and the critical loci are found at nearly the same temperatures as the maximum or minimum.

Materials. H- and D-substituted polystyrenes ($7000 \leq$ MW/amu ≤ 27000) of well-defined molecular weight and polydispersity were obtained commercially and are described in Table 2. The samples were vacuum dried and solutions made up gravimetrically. Isopleths were measured at concentrations varying between 10 and 33 wt %, although for most samples the upper limit of concentration was ≈25 wt %. Solutions at higher concentrations were inconveniently viscous. To determine the amount of polymer in the initial charge to the capillary cell, the residual solution wetting the walls of the syringe was removed by washing with THF, the washings were added to any excess solution left in the weighing bottle, and the entire contents were dried to constant mass. This, together with a value for the initial mass of polymer, provides enough information for an accurate calculation of the charge to the pressure cell. Once charged, the cell contains enough material for runs at two or three dilutions.

Reagent grade propionitrile was dried over molecular sieves, vacuum distilled, rejecting the first and last portions, and stored over molecular sieves. CH_3CD_2CN was prepared by Dr. A. Urbanczyk by an exchange method. NMR and IR analysis shows 75.0% purity (*i.e.* 75% of methylene hydrogen was substituted with D). We are indebted to Dr. Urbanczyk for the use of this material. CH_3CD_2CN was dried and purified by the same method used for CH_3CH_2CN.

3. Results

CP and SP temperatures and pressures are reported as a function of concentration, solvent, and polymer H/D ratio in the supplemental materials. Table 3 presents coefficients of eq 1) for CP isopleths.

$$P_{CP} = A_0 + A_1T + A_2T^2 + A_3T^3 \qquad (1)$$

Ordinarily, in good solvents the upper and lower Θ points are well separated. No minima are observed in the isopleths. As solvent quality deteriorates, however, the upper and lower branches approach one another and eventually merge, thus defining a minimum in the (T,P) demixing isopleth at finite molecular weight (Figure 1b). We find it convenient to single out this point, labeling it a hyperdemixing point for segment fraction ψ, $(T,P)_{hdm,\psi}$. At $(T,P)_{hdm,\psi}$ the upper and lower demixing branches are common, $(\partial T/\partial P)_{hdm,\psi} = 0$, and $(\partial^2 T/\partial P^2)_{hdm,\psi} > 0$. Should the hyperdemixing concentration be the critical concentration, $(T,P)_{hdm,\psi}$ defines a hypercritical point (that point where the upper and lower consolute critical temperatures (USCT and LCST) merge). We will write $(T,P)_{hdm,\psi=\psi_{cr}} = (T,P)_{hcr}$. Obviously, $(\partial T/\partial P)_{hcr,\psi_{cr}} = 0$ and $(\partial^2 T/\partial P^2)_{hcr,\psi_{cr}} > 0$. The relationship between polydispersity and the cloud and shadow and the cloud and spinodal concentrations under noncritical conditions has been discussed by us earlier.[3,4,6] The equilibrium treatment predicts fractionation in segment fraction, segment number, and polydispersity, and a simplified explanation of such effects is diagrammed in Figure 1c. A more complete discussion is found in ref 4.

4. Least-Squares Representation of Results

Luszczyk, Rebelo, and Van Hook[4] have introduced a mean-field model to describe the free energy of polymer/solvent solutions and demixing loci. The approach takes account of the effects of polydispersity using the Ratsch–Kehlen[8] (RK) continuous thermodynamic model and incorporates the theory of isotope effects in condensed phases.[9–11] Other approaches which apply continuous thermodynamics to polymer demixing have been given by Hu, Ying, Wu, and Prausnitz[12] and Mumby, Sher, and van Ruiten.[13]

Following RK, Luszczyk, Rebelo, and Van Hook[4] write expressions for the chemical potential per segment for solvent (A) and polymer (B), which for $r_A = 1$ become

$$\mu_A = \mu_A^* + RT[\ln(\psi_A) + 1 - 1/r^{\#}] + RT \ln f_A \qquad (2)$$

$$\mu_B(r)/r = \mu_B(r)^* + RT[\ln(\psi_B W_B(r))/r + 1/r - 1/r^{\#}] + RT \ln f_B(r) \qquad (3)$$

Here r is the segment number, $\psi = \psi_B = (1 - \psi_A)$ is the segment fraction, and the μ^*'s are standard-state partial molar free energies. Also $(1/r^{\#}) = (1 - \psi)/r_A + \psi/r_B^{\#}$, $1/r_B^{\#} = \int (W_B(r)/r)\, dr$, and $W_B(r)$ is the polymer segment distribution function. If $W_B(r)$ is a Schulz–Flory distribution, a simple result obtains to describe r

Table 1. Listing of (T,P,ψ) Isopleths Investigated for PSh/PNh$_2$, PSh/PNd$_2$, and PSd/PNh Solutions

concn (wt %)	temp range (K)	pressure range (MPa)	no. of points	concn (wt %)	temp range (K)	pressure range (MPa)	no. of points
			A. PS(h)7000 + PN(h)				
13.00	267.2−269.4	0.41−3.57	6	25.00	269.1−271.5	0.67−3.89	5
16.00	268.9−271.2	0.31−3.63	6	26.00	269.5−272.5	0.59−4.43	7
18.00	268.0−270.5	0.51−4.03	6	28.00	269.8−272.8	0.55−4.45	7
19.00	268.9−271.5	0.80−3.99	6	30.00	268.4−271.9	1.02−5.55	7
21.00	268.9−271.5	0.77−4.19	6	33.00	267.9−271.0	0.69−4.55	7
22.00	269.0−271.5	0.74−4.16	6	35.91	268.2−271.0	0.65−4.43	7
24.00	268.9−272.2	0.66−4.93	8				
			B. PS(h)13500 + PN(h)				
16.00	307.3−309.5	1.36−2.57	5	22.56	305.8−309.2	1.42−3.08	5
19.06	308.5−310.4	0.71−2.57	5				
			C. PS(h)16500 + PN(d.75)				
10.00	323.7−463.6	0.47−5.51	6	24.02	330.4−342.9	0.56−4.69	4
14.99	330.3−454.5	0.57−5.25	6	25.33	330.2−454.5	0.64−4.52	6
20.00	330.2−454.5	0.63−5.23	6	26.10	325.3−462.6	0.40−5.68	9
			D. PS(h)22000 + PN(h)				
6.00	331.8−454.4	0.49−3.35	5	18.99	337.0−454.6	0.25−4.93	12
9.00	336.3−454.7	0.87−4.54	8	21.99	337.0−454.4	0.40−4.97	11
10.76	337.3−454.8	0.48−4.72	9	24.99	337.0−454.5	0.30−4.58	11
13.00	337.2−351.1	2.53−4.59	3	27.50	337.1−454.4	0.46−4.27	11
16.00	337.1−454.7	0.18−4.89	11				
			E. PS(h)25000 + PN(h)				
12.45	358.9−438.3	2.45−5.33	12	19.99	366.0−437.5	3.09−5.33	10
14.00	352.1−437.2	1.77−5.18	12	24.59	358.5−437.2	2.40−5.43	11
15.99	366.2−438.0	2.87−5.11	10	27.98	344.8−438.0	0.67−4.18	5
16.87	358.1−437.0	1.98−4.57	11	29.71	345.0−438.3	0.51−4.53	11
17.99	366.0−438.0	3.11−5.31	10				
			F. PS(h)22000 + PN(d.48)				
8.00	357.7−445.3	0.75−4.16	12	17.99	357.8−445.5	2.08−5.60	12
11.01	357.8−445.5	1.81−5.43	12	21.01	357.8−445.5	1.85−5.23	12
12.00	357.8−365.0		2	24.00	357.8−445.5	1.48−4.75	12
14.47	365.0−445.5	2.41−5.21	11	27.26	350.8−445.5	0.56−4.85	13
15.00	357.8−445.5	2.17−5.78	12	30.73	343.8		1
			G. PS(h)22000 + PN(d.64)				
18.00	372.4−419.7	3.72−5.42	7	27.00	365.1−445.6	2.66−5.52	11
20.98	365.0−445.4	3.30−6.15	11	29.64	360.7−454.4	2.33−6.06	13
24.01	365.1−445.5	2.91−5.77	11				
			H. PS(h)22000 + PN(d.75)				
13.99	373.1−446.5	3.47−5.75	10	22.99	372.5−437.2	3.80−6.04	9
17.00	373.1−446.2	3.64−5.83	10	25.88	380.0−436.7	3.72−5.17	8
22.02	372.9−437.4	2.91−5.77	9				
			I. PS(h)25000/PS(d)27000 + PN(h)				
13.00	330.3−454.7	0.39−4.99	10	21.98	334.4−454.4	0.65−5.29	12
15.99	330.3−454.7	0.53−5.36	11	24.99	333.7−458.1	0.17−5.13	10
19.00	330.2−454.6	0.53−5.31	10				
			J. PS(d)27000 + PN(h)				
11.00	298.4−463.5	0.71−4.82	8	19.99	298.7−463.5	0.76−5.19	9
14.01	298.4−463.5	0.57−5.03	9	23.01	294.7−463.9	0.69−5.33	10
16.99	298.5−463.4	0.77−5.17	9	25.81	294.7−463.6	0.57−5.17	10

Table 2. Characteristics of Polystyrene-*h* and Polystyrene-*d* Samples

polymer	M_w	r[a]	M_w/M_n	source[b]
(h_8)PS07	8000	76.8	≤1.09	PC-80314
(h_8)PS13	13500	129.6	≤1.06	PC-30420
(h_8)PS17	16700	160.3	≤1.05	SPP-746
(h_8)PS22	22091	212.1	1.03	PL-20131/2
(h_8)PS25	25000	240.0	≤1.06	PC-30811
(d_8)PS27	27000	240.7	1.06	PL-20632/1

[a] Segment molecular mass = 104.16 for (h)PS and 112.16 for (d)PS. [b] PC = Pressure Chemical Co., PL = Polymer Laboratories, and SPP = Scientific Polymer Products.

fractionation (h is a parameter which depends on polydispersity, $1/h = (\rho_m - 1)$, $\rho_m = M_w/M_n$).

$$\psi_2/\psi_1 = (r_{B,2}{}^{\#}/r_{B,1}{}^{\#})^{(h+1)} \quad (4)$$

The segment molar activity coefficients f_A and $f_B(r)$ may depend on T, P, ψ, $W_B(r)$, and r. If the excess free energy is of the Redlich−Kister form,

$$G^{ex}/R = \psi(1-\psi)[\chi_0(T,P,y_D,z_D) + \chi_1(T,P,y_D,z_D)(1-2\psi) + ...] \quad (5)$$

For a one-term fit, $\ln(f_A) = \chi_0(T,P,y_D,z_D)\psi^2/r_A$ and $\ln(f_B) = \chi_0(T,P,y_D,z_D)(1-\psi)^2/r$.

One might proceed to make an initial guess for a set of adjustable parameters $(\chi_o,\chi_1,\chi_2,..)_0$ to use in the search for fractionations to satisfy the constraints $\Delta\mu_A = (\mu_A(1) - \mu_A(2)) = \Delta\mu_B = (\mu_B(1) - \mu_B(2)) = 0$. Although straightforward in outline, that procedure is tedious to implement because the free energy minima are extremely shallow, especially near extrema. Convergence is slow and we found it impractical to employ this method.

An Approach Based on the Maxwell Criterion. We have proceeded by defining a difference function,

Table 3. Coefficients of Smoothing Parameters (See Eq 1) for Isopleths Listed in Table 1

concn (wt %)	cloud point polynomial constants A_0	$-A_1$	10^2A_2	-10^5A_3	$10^2\sigma$	no. of points	concn (wt %)	cloud point polynomial constants A_0	$-A_1$	10^2A_2	-10^5A_3	$10^2\sigma$	no. of points
					A. PS(h)7000 + PN(h)								
13.00	373.611	1.38520			5	6	25.00	359.122	1.31998			5	5
16.00	383.522	1.42766			5	6	26.00	355.588	1.30279			1	7
18.00	374.520	1.38264			3	6	28.00	360.162	1.31850			7	8
19.00	356.402	1.31027			2	6	30.00	362.269	1.32863			9	8
21.00	371.095	1.36408			6	6	33.00	326.425	1.20181			4	7
22.00	368.025	1.35297			5	6	35.91	370.273	1.36398			2	7
24.00	350.364	1.28451			5	8							
					B. PS(h)13500 + PN(h)								
16.00	177.868	0.570477			4	5	22.56	160.105	0.513600			10	5
19.06	163.383	0.524910			2	5							
					C. PS(h)16500 + PN(d.75)								
10.00	1323.99	9.54429	2.25987	1.75981	31	13	24.02	115.211	0.334772			11	7
14.99	1382.28	9.88384	2.32351	1.79731	5	12	25.33	1233.05	8.75521	2.03972	1.55964	3	11
20.00	1310.54	9.32661	2.18063	1.67560	5	11	26.10	1109.60	7.87253	1.83101	1.39623	11	18
					D. PS(h)22000 + PN(h)								
6.00	1243.16	8.95785	2.11833	1.64487	11	8	18.99	1131.76	8.06981	1.89724	1.46850	5	20
9.00	1079.04	7.64995	1.78364	1.36565	6	17	21.99	1084.88	7.69023	1.79532	1.37780	8	22
10.76	1028.06	7.27153	1.69169	1.29204	8	19	24.99	1077.56	7.64408	1.78504	1.36977	7	22
13.00	978.268	5.41686	0.754392		7	7	27.50	1174.63	8.38594	1.97187	1.52527	6	21
16.00	1230.64	8.83382	2.09321	1.63544	7	20							
					E. PS(h)25000 + PN(h)								
12.45	1049.06	7.25800	1.66205	1.25402	3	29	19.99	1177.44	8.20588	1.89668	1.44788	8	22
14.00	1092.84	7.66469	1.77854	1.36050	5	27	22.00	1038.40	7.16525	1.63924	1.23582	2	20
15.99	1075.65	7.45289	1.71075	1.29501	2	20	24.59	1388.62	9.80769	2.29856	1.78250	6	23
16.87	1062.21	7.42954	1.71953	1.31177	2	20	27.98	608.251	4.20725	0.944047	0.681217	19	9
17.99	990.041	6.79547	1.54387	1.15456	2	22	29.71	1082.04	7.71457	1.81160	1.39730	13	24
					F. PS(h)22000 + PN(d.48)								
8.00	997.036	6.86396	1.55875	1.16342	6	24	17.99	1181.87	8.19096	1.87959	1.42305	4	24
11.01	1053.24	7.23266	1.64196	1.22709	7	24	21.01	1123.59	7.77211	1.77870	1.34189	4	24
14.47	1091.60	7.50818	1.70920	1.28228	3	22	24.00	1076.76	7.41907	1.68882	1.26520	5	24
15.00	1175.52	8.13700	1.86500	1.41017	5	21	27.26	1213.44	8.52231	1.97932	1.51671	5	25
					G. PS(h)22000 + PN(d.64)								
18.00	1121.03	7.65505	1.73380	1.29605	2	13	27.00	1183.23	8.09682	1.83458	1.37061	3	22
20.98	1458.33	10.1329	2.33604	1.78069	7	24	29.64	1247.09	8.56080	1.94495	1.45693	8	27
24.01	1202.44	8.24221	1.87168	1.40214	3	23							
					H. PS(h)22000 + PN(d.75)								
13.99	1381.25	9.51373	2.17627	1.64728	5	22	22.99	1186.73	8.06010	1.81609	1.35092	2	18
17.00	1208.39	8.21812	1.85398	1.38102	3	20	25.88	1278.35	8.75460	1.99076	1.49680	3	15
22.02	1158.47	7.86364	1.77068	1.31613	1	23							
					I. PS(h)25000/ PS(d)27000 + PN(h)								
13.00	1069.17	7.69933	1.82551	1.42290	7	18	21.98	1243.08	8.95690	2.12616	1.66059	15	27
15.99	1016.93	7.27952	1.71368	1.32409	10	19	24.99	1067.48	7.61233	1.78522	1.37477	10	20
19.00	999.366	7.15313	1.68375	1.30071	9	20							
					J. PS(d)27000 + PN(h)								
11.00	1034.85	7.75111	1.88579	1.49517	15	18	19.99	1023.74	7.65411	1.85989	1.47289	11	18
14.01	1046.55	7.83205	1.90526	1.51103	12	17	23.01	832.934	6.19080	1.49096	1.16582	20	23
16.99	1054.33	7.86525	1.90813	1.50931	30	17	25.81	995.027	7.46283	1.81728	1.44137	12	20

$DIFF_k$, between the chemical potentials of each component, k, in the equilibrating phases. From this point, we represent the set of excess free energy parameters $(\chi_0,\chi_1,\chi_2,...)$ with the single unsubscripted symbol χ. At equilibrium $DIFF_k = 0$ for all k.

$$DIFF_k = f(\psi,r,\rho,y_D,z_D,T,P,\chi) = \sum|\mu_k(1) - \mu_k(2)| = 0 \quad (6)$$

We examine the ψ dependence of $f(\psi,r,\rho,y_D,z_D,T,P,\chi)$, holding y_D, z_D, T, and P constant and remembering that any effects of r and ρ have already been taken care of by incorporation of the segment distribution function, $W(r)$, into the equations for phase equilibria. This leads to a further economy of notation, $f(\psi,\chi) = f(\psi,r,\rho,y_D,z_D,T,P,\chi)$. We have chosen the Schulz−Flory distribution for $W(r)$ for the present calculations, but the method can be generalized to other $W(r)$. For near-equilibrium conditions, three roots, a, b, and c, are expected for $DIFF_k$. The innermost and outermost of these, a and c, correspond to physical solutions: they are the cloud and shadow concentrations. Root b has no physical meaning. According to the Maxwell criterion

$$\int_a^b f(\psi,\chi)\,d\psi = -\int_b^c f(\psi,\chi)\,d\psi \quad \text{and} \quad \int_a^c f(\psi,\chi)\,d\psi = 0 \quad (7)$$

The scheme of the calculation is now apparent. Using an initial first guess set of excess free energy parameters $\chi(\chi_0,\chi_1,\chi_2,...)$, $f(\psi,\chi)$ is calculated as a function of ψ over an appropriate range of concentration for each data point. If the result is well behaved, *i.e.* shows three roots, the integrals in eq 7 are evaluated numerically (trapezoid method) and stored. If, in this initial approximation, $f(\psi,\chi)$ for a given data point is not well behaved and does not show three roots (because of a poor initial guess for χ or due to experimental error in

one or more of the independent variables), the integral is numerically evaluated from the starting point, ψ_{CP}, to an arbitrary concentration certain to include the shadow concentration, and the result stored. The objective is to optimize the set of parameters by minimizing the sum of integrals for all data points. Because integration has been replaced by summation, the condition is to find the minumum in the double sum

$$\min = \sum_{i=1}^{n}\sum_{j=1}^{m} w_n f_{n,m}(\psi,\chi)\,\delta\psi \qquad (8)$$

where n is the number of data points, m the number of steps (about 200) in the numerical integration, w_n the statistical weight assigned to the point, and χ the array of fitting parameters. The assignment of weights is a critical step. We note that the size of the integrals in eq 7 increases dramatically (by orders of magnitude) as one moves away from the critical concentration. For this reason, and because the phase equilibrium data near extrema in the demixing curves are experimentally more reliable than data at the extremities, we assigned weights proportional to the reciprocal of the absolute value of the larger half-integral.

The least squares calculation numerically locates the local minimum

$$0 = \sum_{i=1}^{n}\sum_{i=1}^{n} \partial(w_n f_{n,\mathrm{m}}(\psi,\chi))/\partial\psi \qquad (9)$$

and numerically differentiates to obtain a set of linear equations to be solved for $\delta\chi$.

$$0 = \sum_{k=1}^{l}\sum_{i=1}^{n}\sum_{j=1}^{m} \partial^2(w_n f_{n,m}(\psi,\chi))/\partial\psi^2 \qquad (10)$$

Iteration continues with the improved set of parameters defining a new set of Maxwell area integrations, weights, etc. We generally found the best results after three iterations. Weights and integration limits are reset in each cycle so that several iterations are required.

Representation of the $\chi(\chi_0,\chi_1,\chi_2,...)$ Package. We chose the Redlich−Kister formalism to describe the dependence of the χ parameters on experimental variables, writing

$$G^{\mathrm{ex}} = \psi(1-\psi)\sum_{i=0}^{n}\chi_i(1-2\psi)^i \qquad (11)$$

where the χ's are expressed for $i = 0$ as $\chi_0 = \chi_{0,T} + \chi_P P + \chi_r/r + \chi_{y_D} y_D + \chi_{z_D} z_D$, with $\chi_{0,T} = \chi_{0,0;T} + \chi_{0,1;T}T + \chi_{0,2;T}T^2 + ...$, and for $i > 0$, $\chi_i = \chi_{i,0;T} + \chi_{i,1;T}T + ...$, $\chi_P = \chi_{0;P} + \chi_{1;P}P + \chi_{2;P}/T$, and finally $\chi_r = \chi_{0;r} + \chi_{1;r}r + \chi_{2;r}r^2 + ...$ The $\chi_{i,j}$'s may be functions of T, P, r, y_D, and z_D, but not ψ. The objective of the least squares routine is to pick the best-fit set of $\chi_{i,j}$'s. Values of least squares parameters from fits to the data net in the supplemental material are given in Table 4. That set of parameters comprises a reasonably quantitative description of demixing thermodynamics for PS/PN solutions corresponding to the model. In the section which follows, we supplement this parametric description with a discussion of graphical representations of the data.

Uncertainties. The least squares minimization criterion specified in eqs 8−10 is in a way artificial. To compare calculation and experiment, we employed the set of excess free energy parameters $\chi(\chi_0,\chi_1,\chi_2,...)$ to find a calculated equilibrium temperature at the pressure and concentration of each data point and compared it with the observed CP temperature. The goodness of fit is then tested by comparing experimental and least-squares-calculated equilibrium temperatures. It would make equal sense to fix the temperature at the observed experimental value and compare calculated and experimental pressures instead, but we have chosen the first approach as more convenient. We have found that the standard deviation in temperature so calculated, $\delta T_{\mathrm{SD}} = [(T_{\mathrm{lsq}} - T_{\mathrm{exp}})^2/(n-1)]^{1/2}$, levels off to about 2−2.5 K after three or so iterations, and this is the origin of our claim that best fits are found after three iterations.

It is interesting to compare the observed value for δT_{SD} with that expected from an analysis of the expected experimental error. The experimental precision is such that reproducibility of a single data point is on the order of ±0.02 K, ±0.05 MPa, and ±0.001 ψ unit. Polynomial representations of CP data for a single sample are of approximately this precision (see Table 2). The precision on the total data net is more difficult to estimate. Some imprecision creeps in when the ψ dependence is introduced, probably doubling or tripling δT, but the single largest uncertainty is that introduced by forcing a comparison of equilibrium temperatures for polymer samples of different MW and polydispersity, ρ. This is because the relative uncertainties in the segment numbers, r, and especially in $\rho = M_{\mathrm{w}}/M_{\mathrm{n}}$ are relatively large, and $(T,P)_{\mathrm{eq}}$ loci are sensitive to these parameters.[4] Summing up, we think it reasonable to estimate the net contribution of experimental imprecision to δT_{SD} as ≈0.5 K. This estimate is approximately a factor of 5 lower than δT_{SD}(lsq fits), and we attribute the difference to inaccuracies in the model selected to represent $\chi(\chi_0,\chi_1,\chi_2,...)$. That model has been limited to linear representations of the P, and ψ dependences of the χ's, and thus fails to accurately represent the details of curvature in the data net. This is easily seen by comparing calculation and experiment in regions of high curvature (*i.e.* near $(T,P)_{\mathrm{hcr}}$ and $(T,P)_{\mathrm{hcm},\psi}$), where the

Table 4

(a) Least-Squares Parameters of Fit of the PS/PN Data Net from Tables 1 and 3 and the Supplemental Material to the Mean-Field Formalism Described in Eqs 2−5 and 11[a]

parameter	value	units
$\chi_{0,0;T}$	2561.45	J mol^{-1}
$\chi_{0,1;T}$	−6.85980	J mol^{-1} K^{-1}
$\chi_{0,2;T}$	1.69655×10^{-2}	J mol^{-1} K^{-2}
$\chi_{1,0;T}$	−33.9610	J mol^{-1}
$\chi_{1,1;T}$	-5.78192×10^{-1}	J mol^{-1} K^{-1}
$\chi_{0;P}$	−35.3841	J mol^{-1} MPa^{-1}
$\chi_{1;P}$	2.65866×10^{-1}	J mol^{-1} MPa^{-2}
$\chi_{2;P}$	9035.74	J mol^{-1} MPa^{-1} K
$\chi_{0;r}$	−19104.0	J mol^{-1}
$\chi_{1;r}$	70.1035	J mol^{-1}
$\chi_{2,r}$	2.29784×10^{-1}	J mol^{-1}
χ_{y_D}	−133.284	J mol^{-1}
χ_{z_D}	52.0903	J mol^{-1}

(b) Examples of Deviations between Least-Squares Model Predictions and Experiment

solution	(tot syst dev of T)/K	(std dev of T)/K
A. PS(h)7000 + PN(h)	−2.3	1.0
B. PS(h)13500 + PN(h)	2.5	2.5
D. PS(h)22000 + PN(h)	115	3.8
E. PS(h)25000 + PN(h)	530	12

[a] The parameters reported in this section of the table are those found after three iterations (see text).

standard deviations are larger or much larger than average.

In spite of the fact that δT_{SD} might be improved by the addition of higher order terms, we have elected not to take this step because of the uncertainty implied by a more complex model and the additional correlation error introduced into the set of χ's. A more efficient route is to explore different algebraic forms for the representation of the $\chi(\chi_0,\chi_1,\chi_2,...)$ package. We have chosen to defer the lengthy study which that statement implies.

5. Graphical Representations and Discussion of Results

It is useful to present the results of the least squares analysis graphically in order to better appreciate the nature of the phase transition and the quality of the fits. The most interesting part of the diagram is near the hypercritical point where the upper and lower branches join. That part of the diagram is the most sensitive to the choice of the functional form of the least squares fit and the choice of parameters. Most of the discussion which follows will center there.

Figures 2 and 3 show (T,ψ) projections of phase diagrams for PSh/PNh solutions in the hypercritical region as calculated from the least squares parameters reported in Table 4. Figure 2 a compares predicted cloud points for a PS sample of arbitrary segment number, $r = 212.4$, but near the hypercritical value, and at pressures between 0 and 2 MPa. That range of pressure includes P_{hyp} for $r = 212.4$. Similarly, Figure 2b shows predicted cloud points at an arbitrary pressure, $P = 0$, for PS samples over the range $196.8 < r < 212.4$, which range includes r_{hyp} at $P = 0$. Here r_{hyp} is the segment average hypercritical segment-number and is related to the weight-average molecular weight according to M_w /amu $= 104r + 57$ (because the monomer molecular weight is 104 and the chains are *tert*-butyl terminated). Figure 2 clearly demonstrates that the phase diagram is sensitive to P and r near the hypercritical point. To the nearest integer, $r_{hyp,lsq} = 199$ at $P = 0$, and $r_{hyp,lsq} = 212$ at $P = 0.4$ MPa. To reduce clutter in Figure 2 we have not shown shadow, spinodal, or shadow−spinodal loci (information which is also available from the calculation), nor have we plotted experimental data points. Recall that the experiments fixed concentration, segment number, and isotope label and then measured cloud and spinodal $(T,P)_{\psi,y_D,z_D,r}$ isopleths, so plots in the $(T,\psi)_{P,y_D,z_D,r}$ at arbitrary P imply interpolation or preliminary smoothing (see Table 3).

To exemplify the comparison between the least squares model and experiment, Figure 3 shows cloud and shadow, and spinodal and shadow-spinodal loci for PSh/PNh solutions with $r = 212.4$, $\rho = M_w/M_n = 1.05$, and $P = 0.50$ MPa (Figure 3a), and $r = 212.4$, $\rho = 1.05$, and $P = 0.00$ MPa (Figure 3b). Under these conditions, $P_{hyp,lsq} \sim 0.4$ MPa. The polydispersity index, $\rho = 1.05$, is typical of the PS samples employed in this investigation (see Table 2). The cloud point curves for the plots in Figure 3 have been previously shown in Figure 2a.

Figure 3 shows that for our samples, which are of modest polydispersity, only small differences are found between cloud and shadow, and spinodal and shadow-spinodal loci. In such cases, the monodisperse approximation may be appropriate (even though the calculations we have reported in Table 4 take polydispersity into quantitative account). We have previously emphasized the importance of proper treatment of polydispersity in studies of liquid−liquid demixing equilibria,[4] and in a later paper in this series,[14] we will report on experimental measurements of cloud and spinodal loci for samples of widely different polydispersity where the corrections are more important. Information on shadow and spinodal loci is available for all calculations reported in this paper but most often we have chosen not to plot shadow and spinodal loci in order to reduce clutter and enhance clarity. Rather we focus the discussion on cloud points, measured and calculated, in order to make the comparison between experimental measurement and thermodynamic analysis as direct as possible.

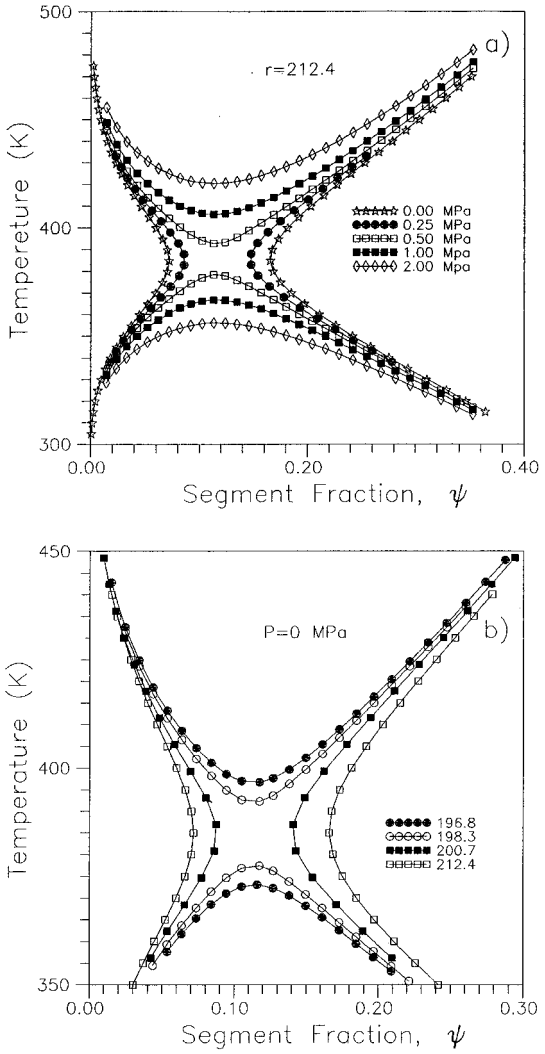

Figure 2. Cloud point loci for PSh/PNh solutions in the hypercritical region calculated from the least-squares parameters in Table 4. (a) Cloud point loci for $r = 212.4$ at several pressures. For pressures below approximately 0.4 MPa, the system is in the hourglass configuration (calculated demixing curves are shown at 0.00 and 0.25 MPa). Above $P = 0.4$ MPa, UCS and LCS demixing branches are observed (UCS/LCS demixing curves are shown at 0.50, 1.00, and 2.00 MPa). (b) Cloud point loci at $P = 0$ for PS of several different chain lengths near the hypercritical value. For $r > 199$ the system is in the hourglass configuration (calculated demixing curves are shown at $r = 200.7$ and $r = 212.4$. Below $r = 199$ UCS and LCS demixing branches are observed (UCS/LCS demixing curves are shown at $r = 198.3$ and 196.8).

Figure 4 makes a direct comparison of the experimentally observed cloud points with the least squares representation. Once again the diagram is in the (T,ψ) plane, this time at two pressures, $P = 0$ (Figure 4a) and $P = 4$ MPa (Figure 4b). The various lines correspond

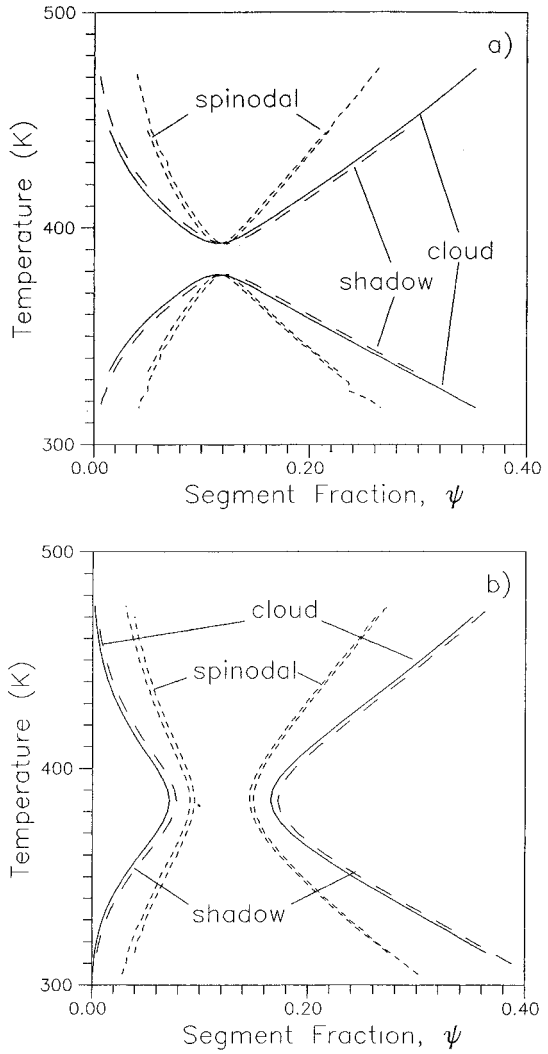

Figure 3. Cloud and shadow, and spinodal and shadow-spinodal loci calculated from the least-squares parameters in Table 4 for (a) $r = 212.4$, $\rho = M_w/M_n = 1.05$, and $P = 0.50$ MPa and (b) $r = 212.4$, $\rho = 1.05$, and $P = 0.00$ MPa. The UCS−LCS/hourglass transition under these conditions occurs around $P = 0.4$ MPa (see text for discussion).

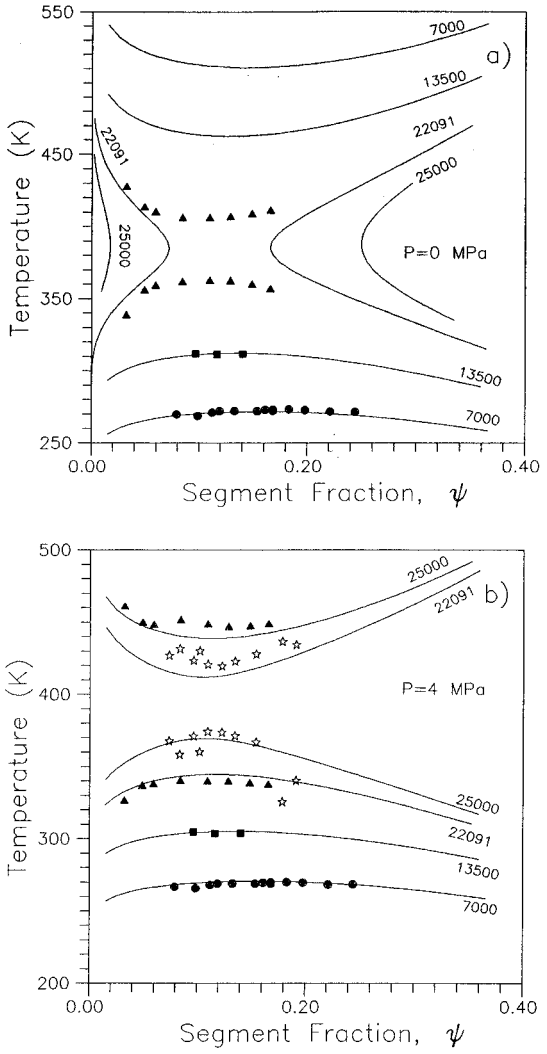

Figure 4. Cloud points in the vicinity of the hypercritical transition at (a) $P = 0$ and (b) $P = 4$ MPa compared with experiment. The curves have been calculated from the least-squares parameters listed in Table 4. The experimental points have been picked from the (T,P) isopleths specified in Tables 1 and 3 (see text for discussion).

to different PS samples [(M_w,r): (7000, 66.8); (13500, 129.3); (22091, 211.9); (25000, 239.8)]. The agreement at 4 MPa is quite good (Figure 4b). Except for several outliers on the UCS branch of the $M_w = 25000$ sample, the agreement is within several K across a reasonably broad range of concentration. At $P = 0$ the agreement at low M_w is good, but the predicted value for r_{hyp} at $P = 0$, 199, is clearly lower than experiment, which is somewhere in the range ($212 < r_{hyp,P=0} < 240$), but nearer the lower end. The experimental data for ($M_w = 25000$, $r = 240$) are in the hourglass configuration (data points not plotted), while those for ($M_w = 22091$, $r = 212$) clearly indicate this solution is in the UCS−LCS configuration at $P = 0$. However, the least squares fit to the model predicts the hypercritical point to have occurred at a lower molecular weight (*vide supra*). The comparison at the two pressures, $P = 0$ and $P = 4$MPa, indicates that the calculated and observed pressure dependences for demixing near the hypercritical point are different by more than the experimental uncertainty. One could bring calculation and experiment into closer agreement by adding additional higher order terms to the model expansion of excess free energy parameters, eq 11, but for present purposes, we feel the agreement shown in Figure 4, which is good but not perfect (*i.e.* not within experimental error), is adequate to demonstrate the usefulness of the present approach. Further refinement should compare changes in the algebraic form of the model and/or the underlying statistical formalism with the simple extension of the present approach to include higher order terms.

Figure 5 shows the effect of methylene deuteration of the propionitrile solvent. Experimental isopleths for solutions of PSh ($M_w = 22091$, $r = 212$, $\rho = 1.03$, $\psi = 0.135$) are shown as a function of solvent deuteration ($y_D = 0$, 0.48, 0.64, and 0.75) in Figure 5a. Under these conditions, the hypercritical pressure increases smoothly from near −1 MPa at $y_D = 0$ to close to 3.6 MPa at $y_D = 0.75$. Although not shown on the figure, Imre and Van Hook[3] have reported experimental points for the $y_D = 0$ isopleth for these solutions under tension (*i.e.* at negative pressure), thus demonstrating the continuity of the equation of state between regions of negative and positive pressure. The hypercritical temperatures also increase with methylene-PN deuteration, but not as markedly as do the hypercritical pressures. Figure 5b shows calculated isopleths for these samples. At $y_D = 0$, as discussed above, the minimum, $(T,P)_{hyp}$, is predicted to lie at a somewhat higher pressure (or, equivalently, a lower chain length, r) than is observed. This

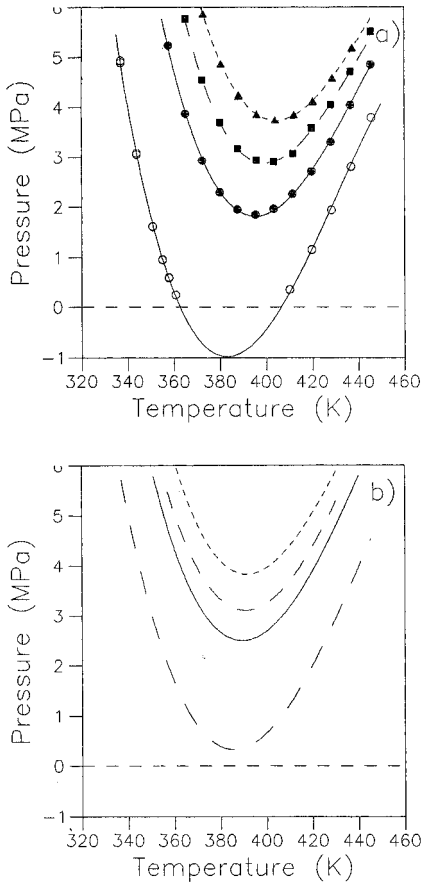

Figure 5. Cloud point loci for solutions of PSh ($M_w = 22091$, $r = 212$, $\rho = 1.03$, $\psi = 0.135$) as a function of methylene deuteration on propionitrile solvent. Reading up, $y_D = 0$, 0.48, 0.64, and 0.75. (a) Experimental data; (b) Calculated from least-squares model parameters reported in Table 4. See text for discussion.

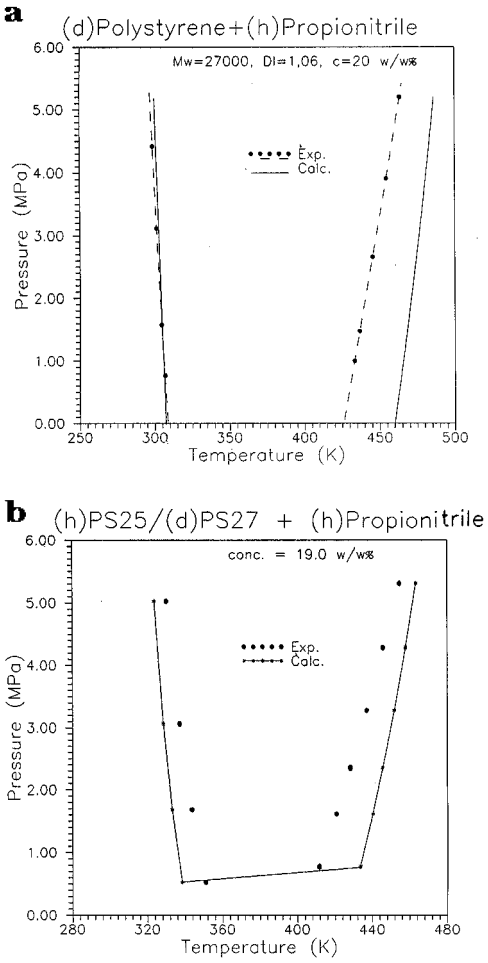

Figure 6. Cloud point loci for solutions of deuteriopolystyrene in protiopropionitrile for $r = 240$. (a) PSd dissolved in PNh ($M_w = 27000$, $r = 240.5$, $\rho = 1.06$, $P = 0$, $\psi = 0.135$). The points and dashed lines represent experiment, and the solid line is calculated from the least squares model in Table 4. (b) Carefully matched mixtures of PSd (as described in (a)) and PSh ($M_w = 25\,000$, $r = 239.8$, $\rho = 1.06$, $P = 0$, $\psi = 0.135$) in propionitrile-*h*. See text for discussion.

pattern holds true as solvent deuteration increases, but the difference is smaller at high y_D. Also the observed trend in T_{hyp}, $[(\partial T_{hyp}/\partial y_{Dcd2})_{\psi_{hyp}} \sim 27$ K], is not well described by the least squares model Figure 5b, because we chose to not incorporate higher order terms to couple the excess free energy parameter which describes the effect of methylene deuteration to temperature and/or pressure. Again, the decision to keep the model usefully simple is only possible at a cost of some loss of detail in the agreement with experiment.

Figure 6 compares experimental data with the least squares fit to the mean-field model for solutions of PSd ($M_w = 27000$, $r = 240.5$, $\rho = 1.06$, $P = 0$, $\psi = 0.135$) and carefully matched mixtures of PSd and PSh ($M_w = 25000$, $r = 239.8$, $\rho = 1.06$, $P = 0$, $\psi = 0.135$) in propionitrile-*h*. Under these conditions, PSh solutions in PNh are in the hourglass configuration, and although not shown on the figure, are in good agreement with the least squares model prediction. Figure 6a compares experimental data for the deuterio polymer with the least squares model which, remember, has been limited to one parameter, χ_{z_D}, to describe polymer deuteration. Good agreement is found along the UCS branch but there is a significant difference between experiment and the least squares model along the LCS branch (*i.e.* at higher temperature). Again, this could be "patched up" were one to introduce a temperature-dependent χ_{y_D} parameter. Figure 6b compares calculation and experiment for the mixed solute system. The quality of the agreement is equivalent to that shown in Figure 6a.

A focal point of these researches has been an interest in the effects of deuteration on the physicochemical properties of solutions, including polymer solutions. We have earlier described a simplified model[1,4] which introduces the theory of isotope effects in condensed phase systems[9−11] into a Flory−Huggins type treatment of polymer solution thermodynamics of the kind employed in this paper. For transfer from the perprotio reference ($y_D = z_D = 0$) to the perdeuteriosolvent state ($y_D = 1$, $z_D = 0$), $\delta\Delta G^{ex} = \psi(\psi - 1)\chi_{y_D}$, $\delta\Delta\mu^{ex}(A) = (1 - \psi)^2\chi_{y_D}$, and $\delta\Delta\mu^{ex}(B) = \psi\chi_{y_D}$, while the transfer free energies to the perdeuterio solute state ($y_D = 0$, $z_D = 1$) are $\delta\Delta G^{ex} = \psi(\psi - 1)\chi_{z_D}$, $\delta\Delta\mu^{ex}(A) = (1 - \psi)^2\chi_{z_D}$, and $\delta\Delta\mu^{ex}(B) = \psi\chi_{z_D}$. The connection between the transfer free energies and molecular properties is commonly discussed using the Bigeleisen AB equation.[9−11] We follow Szydlowski and Van Hook[1] and suggest the major part of the IE's is accounted for in the zero-point energy term and is associated with the frequency shift in the isotope-sensitive carbon−hydrogen (carbon−deuterium) stretching modes as the molecule undergoes its transfer. For PNh *vs* PNd the observed isotope effect, χ_{y_D}, is equivalent to a total 78 cm^{-1} blue shift in the isotope-sensitive methylene stretching vibrations on the transfer from the highly complexed pure solvent reference state to infinite dilution of PN in the polymer standard

state. Similarly, the observed isotope effect on PS deuteration, χ_{yD}, is equivalent to a net ZPE shift of 30 cm^{-1} red shift per monomer unit ($\sim$4 cm^{-1} per PS oscillator) for the transfer from the hypothetical polymer reference state to infinite dilution in PN solvent. These shifts are of reasonable magnitude and sign as compared with results on other studies on polymer solutions[1,4] and with numerous studies in small-molecule systems.[10,11]

6. Conclusion

Experimental CP and SP demixing data have been obtained for polystyrene/propionitrile solutions as a function of pressure, temperature, concentration, segment number, and solute and solvent deuteration. The phase diagrams show upper and lower demixing braches which meet at a hypercritical point which is pressure, isotope, and segment number dependent. A mean-field Flory−Huggins type analysis which takes account of polydispersity according to the Ratsch−Kehlen formalism of continuous thermodynamics was fit to the data using a least squares approach. Cloud point, shadow, spinodal, and shadow-spinodal loci are available from the calculation. The fit, while not quantitative, reproduces the general features of the data, which are complicated.

Acknowledgment. This work was supported by the U.S. Department of Energy, Division of Materials Sciences.

Supporting Information Available: For each polymer/solvent system, at every concentration studied, a listing of temperature and the fluctuation in temperature (in K) over the time of the measurement together with the observed pressure (in MPa) at which the cloud and spinodal points are observed, CP and SP (as obtained from least-squares fits of $1/I_{sc,corr}$ vs P), and the visually observed cloud point pressure, CP_v, as directly "picked off" the computer screen plotting I_{obs} vs P during the experiment (see text) (16 pages). Ordering information is given on any current masthead page.

References and Notes

(1) Szydlowski, J.; Van Hook, W. A. *Macromolecules* **1991**, *24*, 4883.
(2) Szydlowski, J.; Rebelo, L. P.; Van Hook, W. A. *Rev. Sci. Instrum.* **1992**, *63*, 1717.
(3) Imre, A.; Van Hook, W. A. *J. Polym. Sci., Part B: Polym. Phys.* **1994**, *32B*, 2283; **1996**, *348*, 751.
(4) Luszczyk, M.; Rebelo, L. P. N.; Van Hook, W. A. *Macromolecules* **1995**, *28*, 745.
(5) Zywocinski, A.; Wieczorek, S.; Van Hook, W. A. *J. Polym. Sci., Part B: Polym. Phys.* **1995**, *33B*, 595.
(6) Imre, A.; Van Hook, W. A. *J. Phys. Chem. Ref. Data* **1996**, *25*, 637.
(7) Kiepen, F.; Borchard, W. *Macromolecules* **1988**, *21*, 1784.
(8) Ratzsch, M.; Kehlen, H. *Prog. Polym. Sci.* **1989**, *14*, 1.
(9) Bigeleisen, J. *J. Chem. Phys.* **1961**, *34*, 1485.
(10) Jancso, G.; Van Hook, W. A. *Chem. Rev.* **1974**, *74*, 689.
(11) Jancso, G.; Rebelo, L. P.; Van Hook, W. A. *Chem. Rev.* **1993**, *93*, 2645.
(12) Hu, Y.; Ying, X.; Wu, D. T.; Prausnitz, J. M. *Fluid Phase Equilib.* **1994**, *104*, 229; *Macromolecules* **1993**, *26*, 6817.
(13) Mumby, S.; Sher, P.; van Ruiten, J. *Polymer* **1995**, *36*, 2921. Mumby, S.; Sher, P. *Macromolecules* **1994**, *27*, 689.
(14) Luszczyk, M.; Malhotra, R.; Van Hook, W. A., in preparation.

MA9517308